Monthly Notices
of the
ROYAL ASTRONOMICAL SOCIETY

MNRAS **473,** 5617–5629 (2018)
Advance Access publication 2017 October 23

doi:10.1093/mnras/stx2707

Green valley galaxies as a transition population in different environments

Valeria Coenda,[1,2]★ Héctor J. Martínez[1,2] and Hernán Muriel[1,2]

[1]*Instituto de Astronomía Teórica y Experimental (IATE), CONICET–Universidad Nacional de Córdoba, Laprida 854, X5000BGR Córdoba, Argentina*
[2]*Observatorio Astronómico, Universidad Nacional de Córdoba, Laprida 854, X5000BGR Córdoba, Argentina*

Accepted 2017 October 13. Received 2017 October 13; in original form 2017 January 3

ABSTRACT

We present a comparative analysis of the properties of passive, star-forming and transition (green valley) galaxies in four discrete environments: field, groups, the outskirts and the core of X-ray clusters. We construct samples of galaxies from the Sloan Digital Sky Survey in these environments so that they are bound to have similar redshift distributions. The classification of galaxies into the three sequences is based on the UV-optical colour $NUV - r$. We study a number of galaxy properties: stellar mass, morphology, specific star formation rate and the history of star formation. The analysis of green valley (GV) galaxies reveals that the physical mechanisms responsible for external quenching become more efficient moving from the field to denser environments. We confirm previous findings that GV galaxies have intermediate morphologies; moreover, we find that this appears to be independent of the environment. Regarding the stellar mass of GV galaxies, we find that they tend to be more massive in the field than in denser environments. On average, GV galaxies account for ∼20 per cent of all galaxies in groups and X-ray clusters. We find evidence that the field environment is inefficient in transforming low-mass galaxies. GV galaxies have average star formation histories intermediate between passive and star-forming galaxies, and have a clear and consistent dependence on the environment: both, the quenching time and the amplitude of the star formation rate, decrease towards higher density environments.

Key words: galaxies: clusters: general – galaxies: evolution – galaxies: fundamental parameters – galaxies: groups: general.

1 INTRODUCTION

Galaxies in the local Universe can be classified into two broad categories: they are either passively evolving red galaxies with old stellar populations commonly found in high-density regions or blue star-forming galaxies preferentially inhabiting low-density regions. The colour bimodality has been observed from low redshift, $z \sim 0.1$ (e.g. Strateva et al. 2001; Baldry et al. 2004), up to $z \sim 1$ (e.g. Balogh et al. 1998; Im et al. 2002; Bell et al. 2004; Weiner et al. 2005; Willmer et al. 2006). These two populations of galaxies are usually referred to as the *red sequence* (RS) and the *blue cloud* (BC), respectively, in the optical colour–magnitude diagram. This bimodality in galaxy colour and its correlation with galaxy morphology was first noted by Takamiya, Kron & Kron (1995). The advent of the Galaxy Zoo project (Lintott et al. 2008) helped to confirm that this bimodality is not entirely morphologically driven. For instance, Schawinski et al. (2009) found a large fraction of ellipticals in the BC, and Masters et al. (2010) found spirals in the RS.

The origin of the bimodality observed could be due to secular evolution (nature scenario), or to the action of environmental physical processes (nurture scenario). The secular evolution of a galaxy is much more than the mere ageing of its stellar population (Masters et al. 2010, 2011, Mendez et al. 2011). Internal processes of secular evolution in disc galaxies could have important consequences in the process of star formation (i.e. pseudo-bulges; Kormendy & Kennicutt 2004). These are slow processes with time-scales much longer than the dynamic time of a galaxy. The evolution of the stellar mass function of star-forming and quiescent galaxies suggests that galaxies that reach a stellar mass of $\sim 10^{10.8}$ $M_{\odot}$ quench and become quiescent galaxies (e.g. Peng et al. 2010). This effect is known as mass quenching. However, the causes of this decline in star formation are not entirely clear. Among the suggested processes are halo heating (Marasco, Fraternali & Binney 2012) and AGN feedback. Some authors propose AGN feedback as the primary mechanism that originates both the suppression or quenching of star formation in massive galaxies, and the correlation of the central black hole mass with the galactic bulge mass (e.g. Di Matteo, Springel & Hernquist 2005; Martin et al. 2007; Schawinski et al. 2007; McConnell & Ma 2013). We will refer to the many internal

★ E-mail: vcoenda@oac.unc.edu.ar

processes that can quench star formation and are supposed to be independent of the environment, as internal quenching. On the other hand, many quenching mechanisms associated with the environment, which we will refer to as external quenching, have been proposed. One of these mechanisms is ram-pressure stripping of the cold gas in galaxies. This process has a time-scale of a few hundred Myr (e.g. Gunn & Gott 1972; Abadi, Moore & Bower 1999). Galaxy–group interactions such as strangulation can remove warm and hot gas from a galactic halo, cutting off the supply of gas for star formation (Larson, Tinsley & Caldwell 1980; Kawata & Mulchaey 2008). On the other hand, haloes can play a role in diminishing star formation. In massive haloes, shock heating could prevent accretion of cold gas into galaxies, thus inhibiting star formation. Galaxy–galaxy interactions in high-mass systems are frequent and produce morphological transformations (Moore et al. 1996, 1999).

The fraction of red galaxies increases with time (Faber et al. 2007) and, therefore, galaxies must transit from blue to red. These transition galaxies between the RS and the BC are called *green galaxies*, and they inhabit the so called *green valley* (GV) in the colour–magnitude diagram. Several authors have defined the GV using optical colours, preferentially $g - r$, or $u - r$, however, Wyder et al. (2007) found that the UV-optical $NUV - r$ colour provides a more efficient criterion to select GV galaxies. Ultraviolet emission is sensitive to recent star formation, while the r-band is more sensitive to the bulk of the stellar mass, formed over the course of a galaxy's history. Furthermore, Cortese (2012), using UV and mid-IR star formation rates (SFRs), concludes that optical colours are simply not able to distinguish between actively star-forming and passive galaxies.

The intermediate colours of GV galaxies have been interpreted as evidence for recent quenching of star formation (Salim et al. 2007). It has been suggested that, to explain the existence of such populations, galaxy transformations from blue to red must occur on short time-scales (<1 Gyr; Salim 2014), but this picture is still controversial. Schawinski et al. (2014) showed that the colour distributions of GV early-type galaxies can be modelled by a quenching time-scale of ∼100 Myr, while for late-type galaxies a longer time-scale, ∼2.5 Gyr, is required. Recently, Crossett et al. (2017) studied the impact of group environment on star formation in galaxies, finding that group galaxies have shorter quenching time-scales (<1 Gyr) than non-grouped galaxies (∼2 Gyr), thus demonstrating that environment plays an important role in the quenching process. From the theoretical point of view, Trayford et al. (2016) investigated the evolution and the origin of galaxy colours in the EAGLE cosmological hydrodynamical simulation (Crain et al. 2015; Schaye et al. 2015), and found a characteristic time-scale for galaxies to cross the GV of ∼2 Gyr which is independent of both the galaxy mass and the physical mechanism responsible for quenching. They found that galaxies with stellar mass $M_* \leq 10^{10}\,\mathcal{M}_\odot$ in the RS are satellites that got their star formation suppressed by ram-pressure stripping in the outskirts of more massive haloes, while RS galaxies with $M_* \gtrsim 10^{10}\,\mathcal{M}_\odot$ are red, due to the feedback from their central supermassive black hole.

Another scenario has been proposed out of the observations by Salim et al. (2012) and Fang et al. (2012); by studying ultraviolet morphology and star formation histories, these works propose that the GV may be static: most galaxies in the GV are not rapidly moving through it, rather, it is the GV that moves slowly towards lower specific star forming rates.

Moving from the BC to the RS is not the only way for a galaxy to be green; some galaxies may reach the GV from the RS following the resumption of gas accretion from the intergalactic medium (Thilker et al. 2010), or they may be passive galaxies that recently underwent a minor, gas-rich merger (Kaviraj et al. 2009).

GVgalaxies are not a quiescent version of the star-forming galaxies, because they are more centrally concentrated than galaxies in the *main sequence*, which is a region in the stellar mass–specific star formation rate (sSFR) diagram where most star-forming galaxies are found (Brinchmann et al. 2004; Salim et al. 2007; Peng et al. 2010; Elbaz et al. 2011; Leitner 2012). Therefore, the action of simple fading mechanisms, such as gas exhaustion or gas starvation, is not able to fully explain why galaxies could leave the main sequence (Salim 2014). Red galaxies are typically found in high-galaxy density regions, so the environment plays a role in galaxy quenching. In addition, AGN feedback is a viable option (Nandra et al. 2007; Hasinger 2008; Silverman et al. 2008; Cimatti et al. 2013). Recently, Schawinski et al. (2014) concluded that green early-type galaxies require a scenario where both the gas supply and the gas reservoir are destroyed instantaneously, with rapid quenching accompanied by a morphological transformation from disc to spheroid. This gas reservoir destruction could be the consequence of a major merger that, alongside the burst in star formation, fuels the accretion on to the central black hole, resulting in an upsurge of AGN feedback. In contrast, green late-type galaxies are consistent with a scenario where the cosmic supply of gas is shut off, perhaps at a critical halo mass, followed by a slow exhaustion of the remaining gas over several Gyr, driven by secular and/or environmental processes.

Observational results suggest several models of quenching. Therefore, to investigate which quenching mechanisms are more important and the role of the environment, a comparison of GV galaxies in different environments can provide important clues to constrain the proposed scenarios. In this paper, we perform a comparative analysis of a number of properties of galaxies in the field, groups and clusters, searching for systematic differences in the GV, and also in the RS and BC, which could provide clues as to the environmental impact on the evolution of GV galaxies. This paper is organized as follows: in Section 2, we describe the samples of galaxies in X-ray clusters, groups and field; in Section 3, we present our analyses; we discuss our results in Section 4.

2 THE SAMPLES OF GALAXIES

All samples of galaxies used throughout this paper are drawn from the Main Galaxy Sample (MGS; Strauss et al. 2002) of the Sloan Digital Sky Survey's (SDSS; York et al. 2000) Seventh Data Release (DR7; Abazajian et al. 2009). Since the GV is better defined in terms of UV-optical colours, we restrict our analysis to SDSS galaxies that have *NUV* magnitude measured by the *Galaxy Evolution Explorer* (*GALEX*). We take UV data from the final data release of *GALEX*, GR6/7.[1] For each SDSS galaxy, we search for the nearest *GALEX* source that is within 4 arcsec. To avoid the edge of the detectors, where *GALEX* photometry and astrometry degrade, we further restrict to matches that are within 0.6° of the *GALEX* field-of-view centres. In all cases, we use the *NUV* magnitude from the deepest available imaging survey of *GALEX* (AIS, MIS and DIS). SDSS's r-band magnitudes have been corrected for Galactic extinction using the maps by Schlegel, Finkbeiner & Davis (1998). *NUV* magnitudes have been corrected for Galactic extinction using the same extinction maps and assuming $A_{NUV} = 8.87E(B - V)$ (Chilingarian & Zolotukhin 2012). We compute absolute magnitudes assuming a flat cosmological model with parameters $\Omega_0 = 0.3$ and $\Omega_\Lambda = 0.7$ and a

[1] http://galex.stsci.edu/GR6

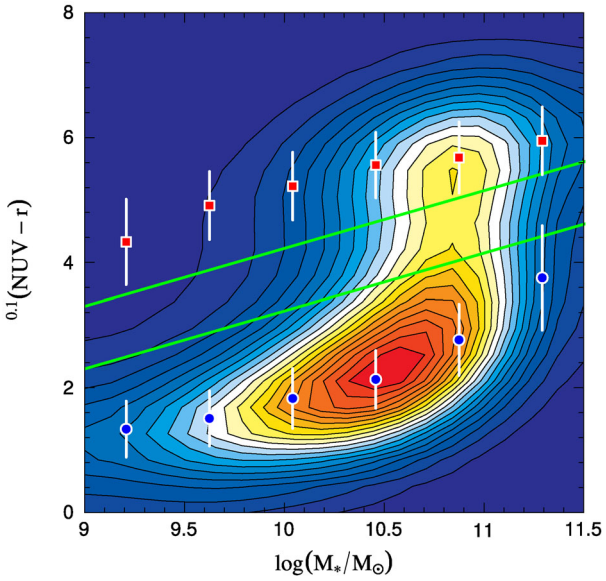

Figure 1. $^{0.1}(NUV - r)$ colour–stellar mass diagram for MGS DR7 galaxies restricted to $z \leq 0.15$. Blue circles and red squares are the centres of the Gaussian functions that fit best the blue and red populations, respectively. Error bars are the corresponding widths. Green lines bound the region we consider as the GV in this paper. See the text for details.

Hubble's constant $H_0 = 100\,h$ km s^{-1} Mpc^{-1}. We have *K*-corrected *NUV* and *r*-band magnitudes to a redshift $z = 0.1$, which roughly corresponds to the peak of the redshift distribution of MGS galaxies, by means of the ZEBRA[2] code (Feldmann et al. 2006). We refer to these band-shifted magnitudes with the superscript 0.1. UV minus optical colours are affected by dust. Following Wyder et al. (2007), we correct the $^{0.1}(NUV - r)$ colour using the empirical dust–SFH–colour relation derived by Johnson et al. (2006). First, we compute the *FUV* attenuation A_{FUV} as a function of $D_n(4000)$ and the uncorrected $^{0.1}(NUV - r)$ from the fits in table 1 of Johnson et al. (2006). Secondly, we calculate the *NUV* and *r* assuming $A_{NUV} = 0.81A_{FUV}$ and $A_r = 0.35A_{FUV}$, which are derived from Calzetti et al. (2000). Unless otherwise specified, colours used throughout this paper are dust-corrected. Stellar masses *Dn*(4000) and sSFRs have been taken from the MPA-JHU catalogue (Kauffmann et al. 2003; Brinchmann et al. 2004). All magnitudes are in the AB system.

The GV is the region that lies between the red sequence and the blue cloud in the colour–magnitude or the colour–stellar mass diagram. These two sequences bounding the GV depend on mass (or luminosity), and so does the GV. We show our definition of GV in the colour–mass diagram of Fig. 1, where we include all MGS DR7 galaxies restricted to $z \leq 0.15$ which have measured *NUV*-band photometry. To define the GV in this diagram, we proceed as follows: (1) We split the galaxies into seven bins of stellar mass, ranging from 10^9 to 3.2×10^{11} M$_\odot$; (2) For each stellar mass bin, we consider the $^{0.1}(NUV - r)$ colour distribution, and fit Gaussian functions separately to both the blue and the red populations. To avoid contamination from the GV in the fits, we use only those points in the colour distribution which lie no further red (blue) than 0.5 mag of the blue (red) peak. We show in Fig. 1 as blue/red points the centres of the Gaussian functions and as white error bars the corresponding widths; (3) We fit straight lines to the position of the peaks of the blue and red populations as a function of mass. It is clear from Fig. 1 that the blue peaks could be described by a different functional form, but we consider this to be beyond the scope of this paper; (4) We define the GV on the colour–mass diagram as those galaxies lying in the region defined by

$$^{0.1}(NUV - r)(M_*) = 0.92 \times \log(M_*) - 5.52 \pm 0.5. \quad (1)$$

The slope of these straight lines is the mean between the slopes of the fits to the blue and red peaks. We have chosen the zero-point in order to define a 1 mag wide strip bounded by the two sequences. This also defines the passive sequence (PS) and the star-forming sequence (SFS), as those galaxies lying above or below the GV, respectively.

Our goal is to perform a suitable comparison of GV galaxies in different environments. Any differences in the populations of GV galaxies due to different environmental effects could be spotted only if the samples of GV galaxies in the environments explored here can be directly compared. Our samples of galaxies in X-ray clusters, groups and in the field were carefully selected to have similar redshift distributions.

2.1 The sample of galaxies in X-ray clusters

Our sample of galaxies in X-ray clusters has been drawn from two sources: the C-P04-I sample of Coenda & Muriel (2009) and the C-B00-I sample of Muriel & Coenda (2014). The former was constructed from the ROSAT-SDSS Galaxy Cluster Survey of Popesso et al. (2004), and the latter from the Northern ROSAT All-Sky Galaxy Cluster Survey of Bohringer et al. (2000), and comprise 49 and 55 clusters, respectively, in the redshift range $0.05 \leq z \leq 0.14$. Galaxies belonging to the clusters in these samples were identified using the same procedure over the DR7 MGS. The authors identified cluster members in two steps. First, they used a friends-of-friends (Huchra & Geller 1982, hereafter *fof*) algorithm that uses the linking parameters and modifications introduced by Díaz et al. (2005). Secondly, they performed eyeball examinations of the structures detected by *fof*. From the redshift distribution of galaxies, they determined the galaxy members from line-of-sight extension of each cluster. By visually inspecting every cluster, the authors excluded systems that have two or more close substructures of similar size in the plane of the sky and/or in the redshift distribution. Using the galaxy members identified this way, the authors computed the cluster physical properties: line-of-sight velocity dispersion, virial radius and mass. Clusters in the C-P04-I sample have a mean virial mass of 7×10^{14} M$_\odot$, a mean virial radius of $1.75h^{-1}$ Mpc and a mean line-of-sight velocity dispersion of 715 km s^{-1}. Clusters in the C-B00-I sample have a mean virial mass of 9×10^{14} M$_\odot$, a mean virial radius of $1.83h^{-1}$ Mpc and a mean line-of-sight velocity dispersion of 820 km s^{-1}.

We include in our sample of galaxies in X-ray clusters, all galaxies in the C-P04-I and C-B00-I clusters that have *GALEX NUV* photometry with the restrictions explained above. Among the three environments explored in this paper, the sample of galaxies in X-ray clusters is, by far, the sparsest, accounting for 4040 galaxies. Thus, this sample will, henceforth, define the redshift distribution that our samples of field and group galaxies must have. The redshift distribution of cluster galaxies can be seen in Fig. 2.

[2] Zurich Extragalactic Bayesian Redshift Analyzer, http://www.exp-astro.phys.ethz.ch/ZEBRA

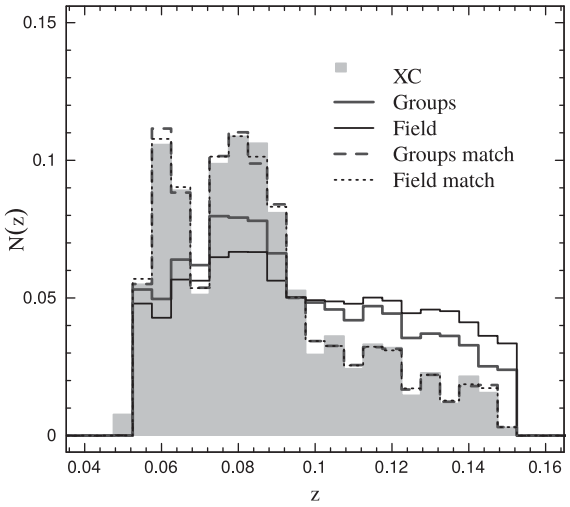

Figure 2. Normalized redshift distribution of our samples of galaxies in X-ray clusters (shaded grey area), groups (grey solid line) and field (black solid line). Dashed and dotted lines show the redshift distribution of galaxies in groups and in the field, respectively, restricted to have redshift distributions similar to that of galaxies in X-ray clusters as described in the text. Kolmogorov–Smirnov tests comparing these distributions with that of the X-ray cluster galaxies confirm that they are consistent with being drawn from the same underlying distribution.

2.2 The sample of galaxies in groups

We draw our sample of galaxies in groups from the sample of groups identified by Zandivarez & Martínez (2011, hereafter ZM11) in the SDSS DR7 MGS. Briefly, they use a standard *fof* algorithm to link galaxies into groups by means of a redshift-dependent linking length. ZM11 split merged systems and cleaned up spurious member detection through a complementary identification procedure, using a higher density contrast in groups with at least 10 observed members (Díaz et al. 2005). Virial masses are computed from the virial radius of the systems and the velocity dispersion of member galaxies (Limber & Mathews 1960; Beers, Flynn & Gebhardt 1990). Groups in the ZM11 sample have a mean virial mass of $2.1 \times 10^{13}\,\mathrm{M}_{\odot}$, a mean virial radius of $0.9h^{-1}$ Mpc and a mean line-of-sight velocity dispersion of 193 km s^{-1}. The catalogue of ZM11 includes 15 961 groups with more than four members, adding up to 103 342 galaxies. We refer the reader to ZM11 and references therein for further details of group identification.

From the original sample of ZM11, we randomly choose among galaxies with *NUV* photometry, with a Monte Carlo algorithm that results in a subsample of group galaxies that have a similar redshift distribution of that of our sample of galaxies in X-ray clusters. This subsample comprises 17 797 galaxies. The redshift distribution of this sample of group galaxies is also shown in Fig. 2.

2.3 The sample of field galaxies

Out of the remaining MGS galaxies that were not included as cluster galaxies or as group galaxies by ZM11, and which have *NUV* photometry, we randomly select as many objects as we can, as long as they have a similar redshift distribution to the sample of galaxies in X-ray clusters, using the same algorithm we use for constructing the sample of group galaxies. This subsample comprises 92 246 galaxies. The redshift distribution of this sample of field galaxies is compared to that of X-ray cluster galaxies and group galaxies in Fig. 2. The samples of clusters and groups used in this paper, are, by construction, not volume complete. Therefore, there are galaxies that belong to clusters and groups that were not identified as such, and thus, they might be contaminating our sample of field galaxies. There is no safe way to exclude these interlopers from our field sample, however, they should be outnumbered by actual field galaxies. Our results regarding field galaxies should be read taking this into account.

3 COMPARING PS, GV AND SFS GALAXIES IN DIFFERENT ENVIRONMENTS

This paper aims to perform a comparison of the properties of galaxies in the PS, the GV and the SFS, in four discrete environments: field, groups and the two in X-ray clusters. The environment itself varies dramatically inside X-ray clusters; the outskirts of these systems are very different from their innermost regions. Therefore, in our analyses, we further distinguish between galaxies located in two regions within clusters: cluster core ($r/r_{200} \leq 0.5$, hereafter $\mathrm{XC_{in}}$) and the outskirts of clusters ($r/r_{200} > 0.5$, hereafter $\mathrm{XC_{out}}$), where r_{200} is the radius that encloses a density 200 times the mean density of the Universe.

In Fig. 3, we show the UV-optical colour–stellar mass diagram of galaxies in the four environments, and the normalized distributions of ${}^{0.1}(NUV - r)$ colour. We include in this figure only those galaxies that have a minor-to-major axis ratio $b/a > 0.45$. The justification for this cut-off is explained later in the section. In this figure, a gradual transition is observed, from the field, which is largely dominated by SFS galaxies, to the inner regions of clusters, where most of the galaxies are in the PS.

We use the morphological classifications taken from the Galaxy Zoo Project (Lintott et al. 2008) to analyse early- and late-type galaxies. Briefly, each galaxy in the Galaxy Zoo Project received several, independent morphological classifications, each performed by a different user. These classifications were processed into raw likelihoods P for every galaxy of a particular morphological type (elliptical, spiral, merger and *don't know*), directly from the ratio of the number of classifications as being of that type to the total. Throughout this paper, we use the probabilities P_{E} (elliptical) and P_{SP} (spiral) corrected after the de-biasing procedure of Lintott et al. (2011). The elliptical class contains galaxies with elliptical morphology and the majority of S0 galaxies, therefore we refer to it henceforth as the early-type class (ET). The spiral classification contains galaxies with different directions and orientation of the spiral arms, and we refer to it as late-type galaxies (LT). As Bamford et al. (2009), we use the raw measures likelihood to weight each galaxy in the statistics by its probability of being either elliptical or spiral, instead of classifying all galaxies into two types defined by a certain likelihood threshold. Hereafter, when we mention our results concerning early or late types, we mean that in the statistics we have used the likelihood P_{E}, or P_{SP}, as a weight. This has the advantage that it retains more information than thresholding, and all galaxies can be included, but it cannot provide classifications for individual objects.

We show in Fig. 4 the normalized distribution of the best model r-band ratio of the axis b/a, as provided by the SDSS data base, as a function of the environment, for all late- and early-type galaxies. Edge-on galaxies have $b/a = 0$ which means an inclination of 90°. Late-type green galaxies are predominantly edge-on galaxies, independently of the environment considered. Edge-on systems darken the ultraviolet radiation due to the presence of dust, shrouding the star formation and, therefore, affecting the colour of the galaxy itself. Although we have corrected colour for dust, hereafter we only

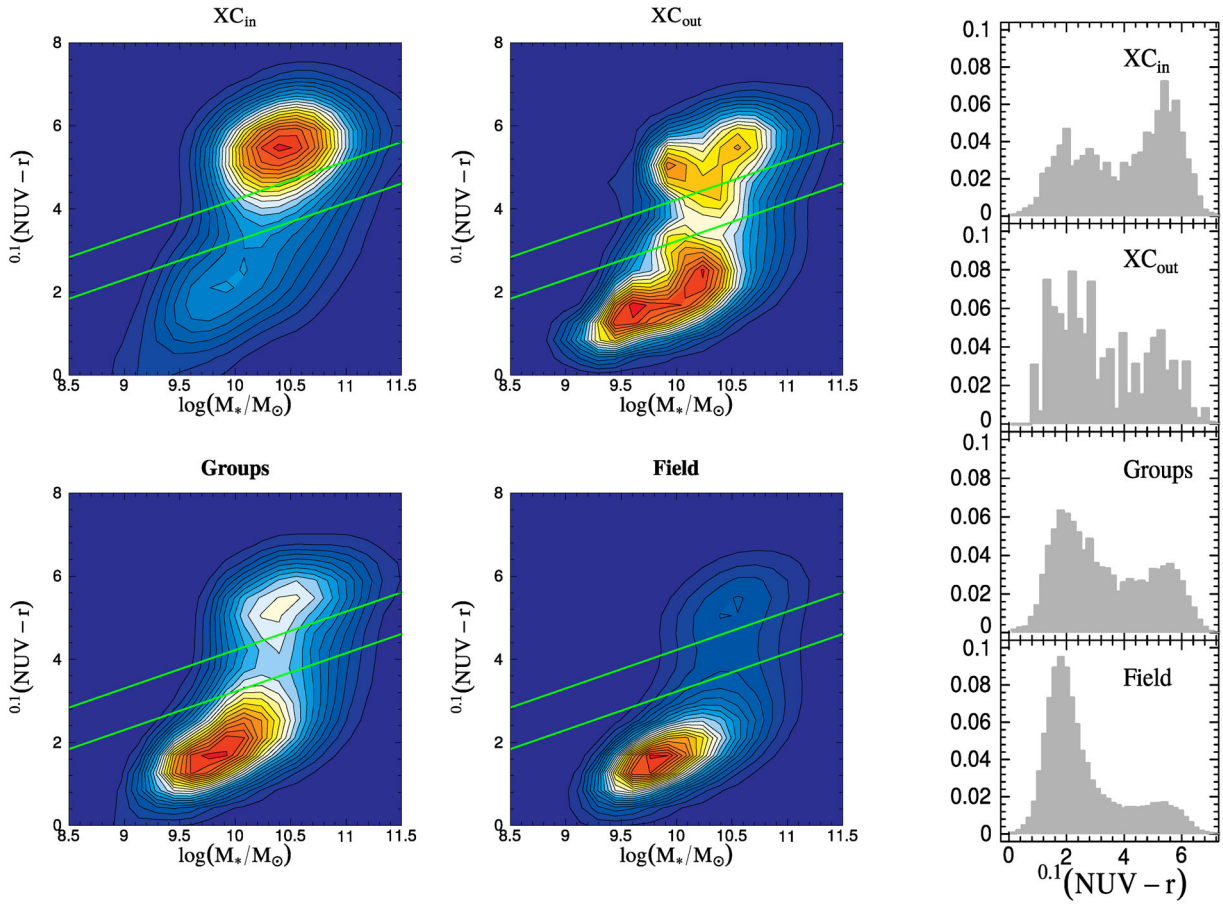

Figure 3. UV-optical colour–mass diagram. Contours indicate increasing density from *blue* to *red*. Top left: galaxies in the inner regions of X-ray clusters. Top right: galaxies in the outskirts of X-ray clusters. Bottom left: galaxies in groups. Bottom right: field galaxies. Horizontal dashed lines define the three sequences (see the text). To the right side of each panel the corresponding $^{0.1}(NUV - r)$ distributions are shown.

consider galaxies with $b/a \geq 0.45$, to avoid objects that could be strongly affected by dust and thus have unreliable UV photometry. This threshold is shown in dashed line in Fig. 4. Other authors have taken into account this source of bias. For instance, Fang et al. (2012) use a threshold of $b/a = 0.65$ to select face-on galaxies. Imposing a cut-off in the axis ratio implies that more spirals are removed than ellipticals. Despite Fig. 4 showing that the distribution of the axis ratios has a small variation with the environment and the star formation classification, we can safely assume that this cut will not introduce major biases in our comparative analyses below.

3.1 Morphology

The upper (lower) panel of Fig. 5 shows the weighted median probabilities P_E (P_{SP}) of galaxies in the different environments and sequences considered. Vertical error bars represent the 25th and 75th percentiles. We include in this figure only galaxies more massive than $10^{9.8}\,M_\odot$. The justification for this cut-off is explained in the next section. Galaxies in the PS have the highest (lowest) median values of P_E (P_{SP}), and they are almost independent of the environment. GV galaxies have median values of P_E and P_{SP} in between those of galaxies in the SFS and the PS, although closer to the values of the PS. The morphology of GV galaxies is also nearly independent of the environment, with the possible exception of the inner region of clusters, where we find that the median values, P_{SP}, in the GV and the PS are very similar. The intermediate morphologies of GV galaxies have been reported by other authors (e.g. Schawinski et al. 2014). Schiminovich et al. (2007) found that GV galaxies have Sérsic indices that are halfway between those of galaxies in the PS and the SFS. Mendez et al. (2011) also found that GV galaxies are intermediate between red and blue galaxies, in terms of concentration, asymmetry and morphological type. Our results confirm these findings, with the exception of galaxies in the inner region of clusters, where few green spirals are found. If there is an effect, it might be an indication that, in the inner region of clusters, both the quenching and the morphological transformation times are shorter than in other environments.

3.2 Stellar mass

In Fig. 6, we compare the normalized stellar mass distributions of galaxies in the PS, the GV and the SFS. First of all, we note that low-stellar mass galaxies are only present in the SFS sub-sample. This is basically due to sample construction: we require that all galaxies in our samples have *NUV* photometry, which implies that for a galaxy to be included in our samples, it must be brighter in *NUV* as its stellar mass is smaller, so as mass decreases, the fraction of SFS galaxies increases to the detriment of the other sequences. Although our samples are not volume-complete, the selection is identical across environments. Therefore, at a fixed stellar mass, it is appropriate to compare the fraction of SFS, GV and PS in different environments. Since there is a lack of galaxies at the low end of the

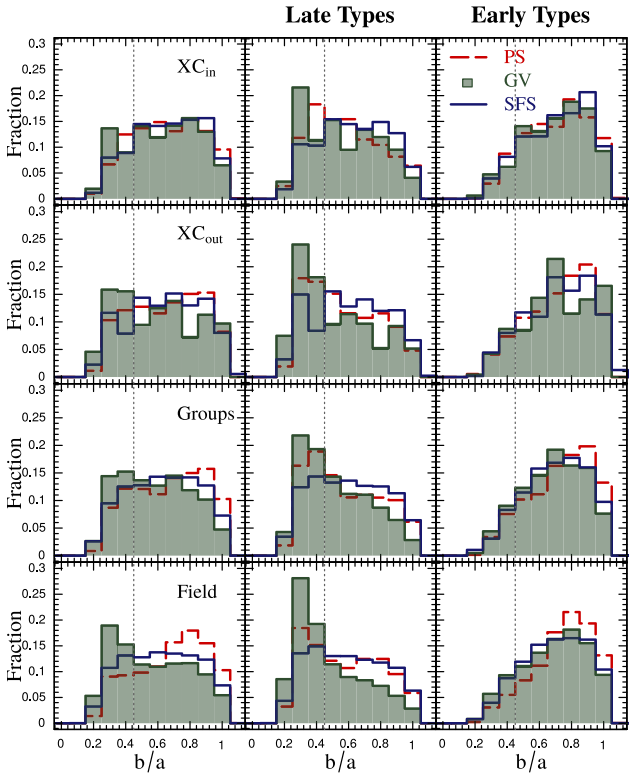

Figure 4. Normalized distribution of a r-band minor-to-major axis ratio b/a as a function of the environment. Dashed lines show the cut $b/a \geq 0.45$ we use to remove dusty edge-on star-forming galaxies. Galaxies in the PS are shown in *red lines*, the GV as a *shaded green area* and the SFS in *blue lines*.

distribution in the GV and the PS, for subsequent analyses we only consider galaxies with $\log(M_*/\mathrm{M}_\odot) \geq 9.8$, in order to have a fair comparison between environments at the low-mass end. After this cut-off, in every binned statistics we have more than 10 galaxies per bin. This threshold is shown in Fig. 6 as vertical dotted lines. After the cut-offs in b/a and stellar mass, the samples of field, group and cluster galaxies comprise 60 553, 12 943, and 3007 objects, respectively.

We find that, with the exception of early type GV galaxies in Groups and XC$_{in}$ (60 per cent probability for the null hypothesis), there is no sequence showing similar mass distributions in different environments. To further explore differences in the GV, in Fig. 7 we compare the stellar mass cumulative fraction of GV galaxies for the four environments considered. We note that, in the field, GV galaxies are slightly more massive than in other environments. This difference is larger for LT galaxies; nevertheless, it is also observed for ET. If internal quenching is the main driver of the transformations of galaxies in the field, it will preferentially affect high-mass galaxies (Peng et al. 2010), while in groups or clusters the environmental effects will also transform lesser massive galaxies. The highest cumulative fraction of low-mass GV galaxies occurs in the outskirts of clusters (orange line in Fig. 7), suggesting that this environment is particularly efficient in transforming these galaxies.

3.3 The relative abundance of the sequences

The ability of the different environments to transform galaxies can be studied by analysing the fraction of objects with different levels

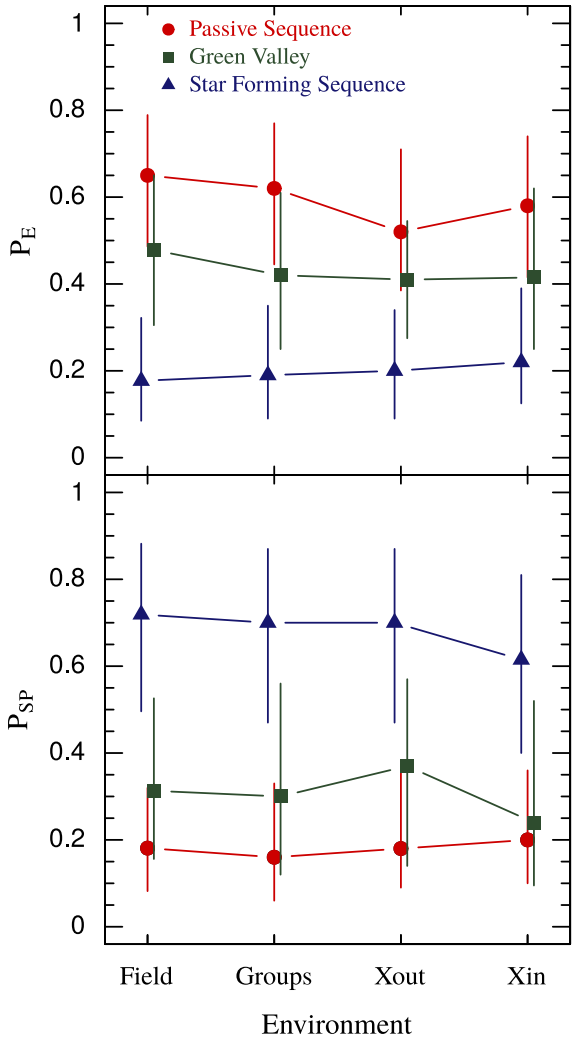

Figure 5. Weighted median probabilities of being elliptical (upper panel) and spiral (lower panel) as a function of environment. Vertical error bars are the 25 per cent and 75 per cent percentiles. GV (SFS) points have been shifted in 0.05 (−0.05) on the x-axis.

of star formation activity as a function of the stellar mass. In Fig. 8, we show the fraction of PS, GV and SFS galaxies as a function of the stellar mass and the environment. At fixed mass and environment, the sum of the fraction of galaxies in all three sequences equals 1. Left column shows the fraction of galaxies irrespective of their morphological type, central column considers late types and right column early types. Recall that the number of galaxies remains the same across columns, since late- and early-types fractions refer to the same galaxies weighted by their likelihood of being either late or early types. As an example of the robustness of the statistics in this figure, the bin with the lowest number of galaxies is the highest mass bin of the XC$_{out}$ environment, which contains 106 galaxies: 44 in the PS, 41 in the GV and 21 in the SFS. Hereafter, all error bars are computed by the bootstrap resampling technique, unless otherwise specified. As expected, the fraction of galaxies in the PS grows with M_* and the opposite behaviour is observed for galaxies in the SFS. Although the same behaviour is observed in all the environments probed, the relative fractions strongly depend on the environment and the morphological type. A different trend is observed in the GV where, with the exception of field galaxies, the fraction of galaxies remains nearly constant with M_*.

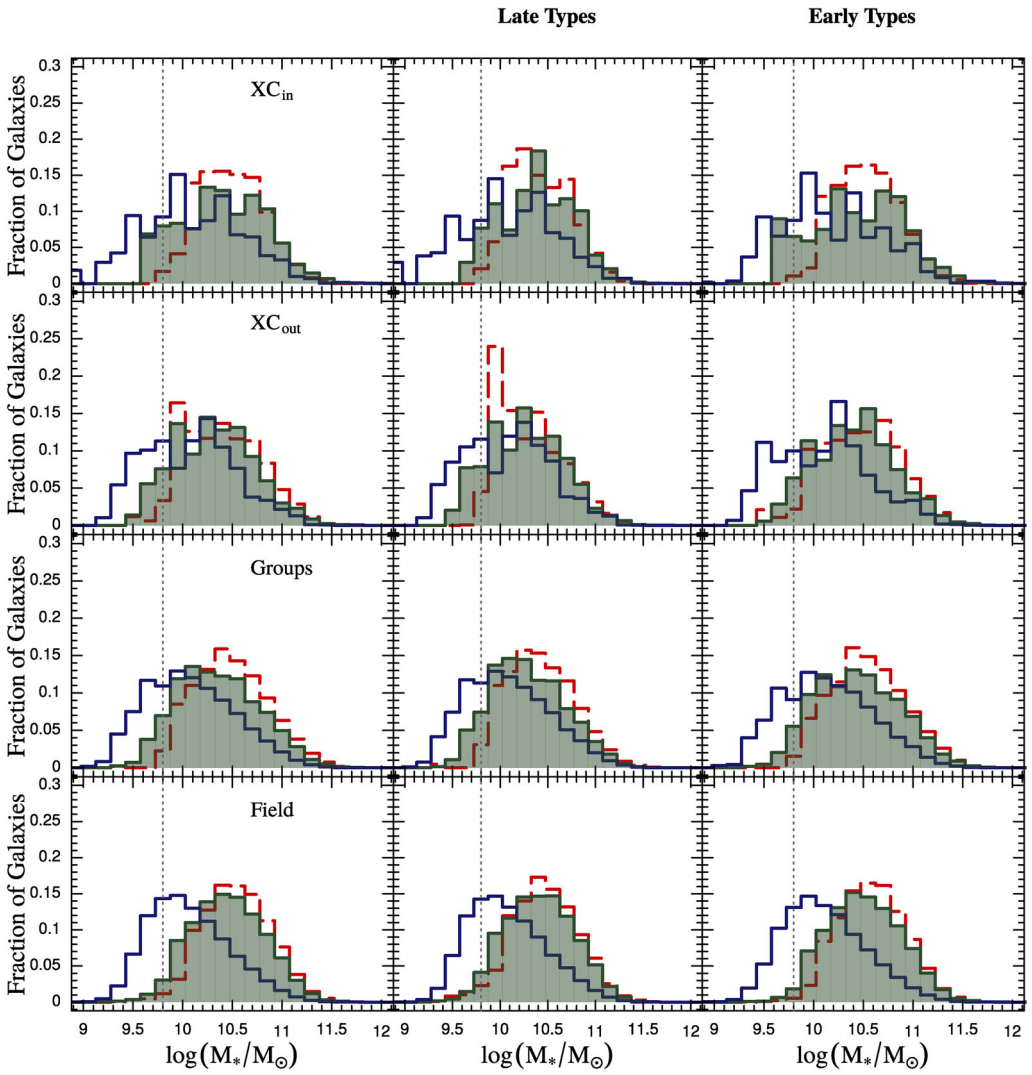

Figure 6. Normalized distribution of stellar mass (MPA-JHU catalogue) for PS, GV and SFS. Colours are as in Fig. 4. Left column: all galaxies, central column: late-type galaxies and right column: early-type galaxies.

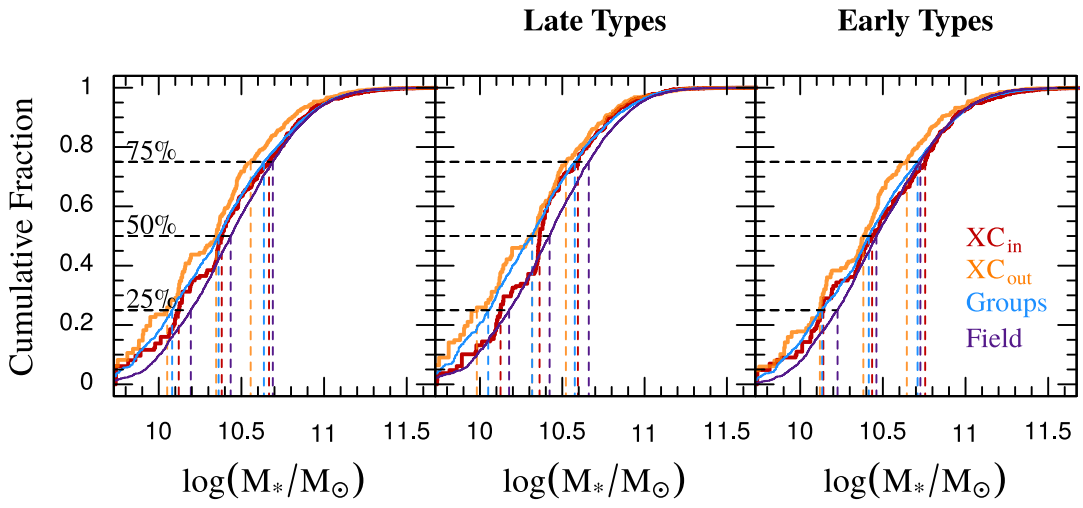

Figure 7. Cumulative fraction of stellar mass for GV galaxies: left-hand panel corresponds to all galaxies, central panel to late types and right-hand panel to early types. Dashed lines represent 25 per cent, median and 75 per cent quartiles of the stellar mass.

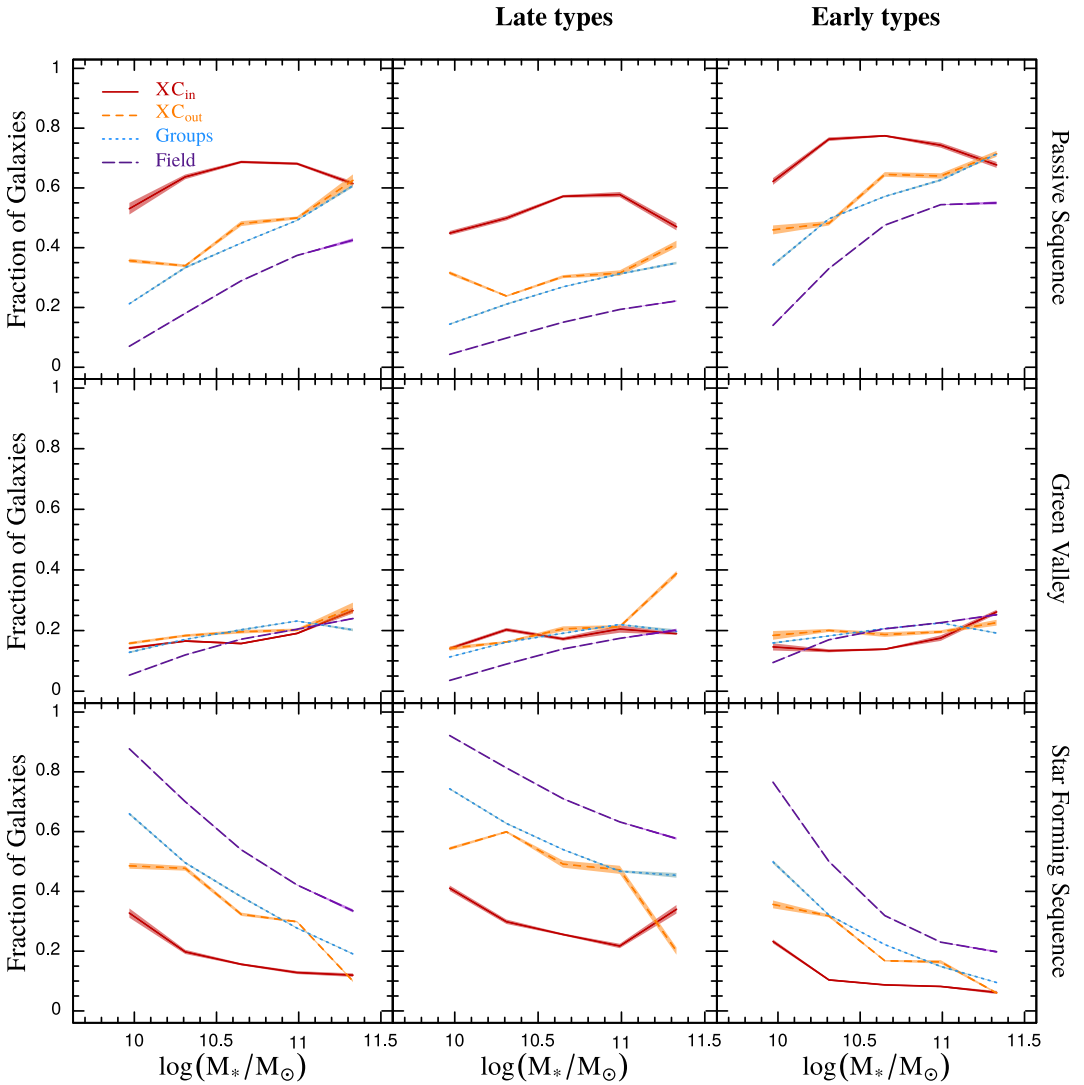

Figure 8. Fraction of galaxies as a function of stellar mass and environment. Left column: all galaxies irrespective of their type, central column: late-type galaxies and right column: early-type galaxies. Upper panels correspond to PS galaxies, middle panels to GV, while the bottom panels represent the SFS. Vertical error bars were computed by using the bootstrap resampling technique.

The fraction of galaxies in the PS is shown in the top row of Fig. 8, where we can see that the highest values are found in the inner region of X-ray clusters. Galaxies at the outskirts of clusters and in groups have very similar fractions, not only in the PS, but also in the GV and the SFS. The lowest relative fraction of galaxies in the PS corresponds to the field, and is nearly zero at the lowest mass bin. For this bin, a low value is also observed for field galaxies in the GV, indicating that a higher density environment is necessary in order to transform galaxies with $M_* \sim 10^{10}\,\mathrm{M}_\odot$. It can also be seen in Fig. 8 that the fraction of high-mass galaxies in the PS is extremely high and similar in galaxy systems (XC$_{in}$, XC$_{out}$ and groups). This result suggests that massive galaxies do not need the extreme conditions of cluster cores to complete their transformation from the SFS to the PS. In the bottom row of Fig. 8, we show the relative fraction of SFS galaxies as a function of stellar mass. The abundance of these galaxies also depends on the environment and, again, XC$_{out}$ and groups have similar values.

In the central row of this figure, we show the fraction of GV galaxies as a function of M_*. With the exception of field galaxies, the GV is populated by objects that show a weak dependence on stellar mass, environment and morphological type. On average, the fraction of galaxies in the GV is ∼20 per cent. It is worth noticing that this is also the case for galaxies in the cluster core, where the reservoir of galaxies to be quenched is quite small. The lack of a strong dependence of the fraction of galaxies in the GV with M_* could be the result of two opposite effects: an increase in the likelihood and/or relative strength of quenching processes as M_* grows, and a decrement with M_* of the number of galaxies in the SFS to be quenched. The population of field galaxies in the GV grows, with the stellar mass being nearly zero for the lower bin of M_*, similar to what was observed for galaxies in the PS.

3.4 The sSFR as a function of stellar mass

In Fig. 9, we show the median sSFR, as a function of the stellar mass for PS, GV and SFS galaxies. In the case of star-forming galaxies, this is known as the *main sequence* (Brinchmann et al. 2004). To facilitate the comparison, in this figure, we include, in the denser environment panels, the trends of galaxies in the field as dashed lines. Clearly, sSFR anticorrelates with M_*, which may be a

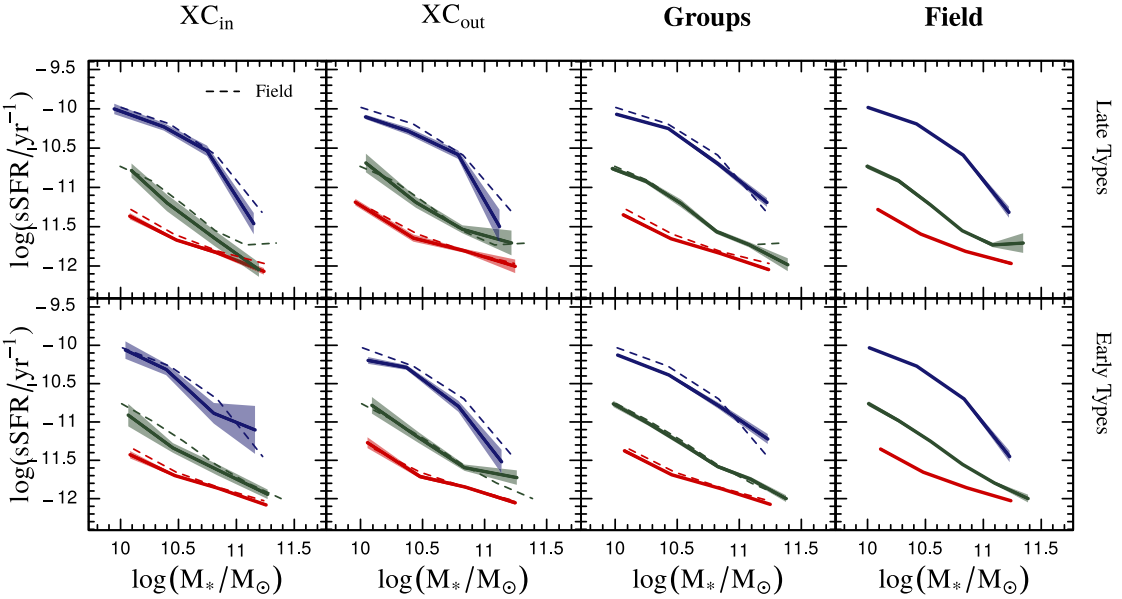

Figure 9. The sSFR as a function of stellar mass for each environment. Top panels correspond to late-type galaxies and bottom panels to early-type galaxies. For a reference, we include the field values as dashed lines in the first three columns. Colours and lines are as in Fig. 4. Error bars were obtained by the bootstrap resampling technique.

consequence of the well-known increase in bulge mass fractions (i.e. portions of a galaxy which do not form stars) with M_* (Abramson et al. 2014). Fig. 9 shows that the sSFR–M_* relation in the GV is far from the main sequence. Both late- and early-type galaxies in the GV are also off the main sequence. The PS of galaxies lies further off the main sequence than green galaxies. We find no evidence of an environmental dependence of the sSFR–stellar mass relation.

3.5 The history of star formation in the inner regions of galaxies

The VErsatile SPectral Analysis (VESPA) catalogue (Tojeiro et al. 2007, 2009) provides a high-resolution star formation history (SFH), which covers the entire age of the Universe by means of 16 time ages, equally spaced in logarithm of time. VESPA SFHs are derived from SDSS spectroscopy, therefore they are a measure of the SFH in the inner parts of galaxies. Therefore, the results of this section concern only central processes. The authors of VESPA warn that their high-resolution SFHs should be used carefully, because they are not generally reliable in a single object basis (Tojeiro et al. 2009). However, these SFHs can be used to perform statistical studies involving several individual objects. We have chosen VESPA's `runID1` model for our computations. This model uses Bruzual & Charlot (2003) spectral synthesis populations and considers a one-parameter dust model, which does not consider extra extinction for younger stellar populations. Since we are interested in studying the overall history of stellar build-up in our galaxies, adopting a two-dust model that gives a special treatment to a young stellar population would not result in an improvement of the resulting SFHs. We have checked that there are no qualitative variations in the results that follow if we use either two-dust models or Maraston (2005) spectral synthesis population models (i.e. VESPA's `runID2`, `runID3` and `runID4` models).

In this part of our analysis, for each sequence and environment, we stack the galaxies into three bins in stellar mass, equally spaced in logarithm of mass, in the range $9.8 \leq \log(M/\mathrm{M}_\odot) \leq 11.5$, and compute an averaged SFH. We basically construct the average SFH of all the stellar mass formed by the galaxies in the bin. Let us consider the k-th bin, which contains N_k galaxies with stellar masses M_i in the range $M^{(k)}_{\rm min} < M_i \leq M^{(k)}_{\rm max}$. Let $m_i(t_j)$ be the stellar mass formed by the galaxy i in the age t_j, thus the total amount of stellar mass formed by this galaxy throughout its lifetime will be[3] $M_i^T = \sum_{j=0}^{15} m_i(t_j)$. The fraction of stellar mass formed in the age j, relative to the total mass amount of mass formed at all ages, by all galaxies stacked in the bin is

$$f_k(t_j) = \frac{\sum_{i=1}^{N_k} m_i(t_j)}{\sum_{i=1}^{N_k} M_i^T}. \quad (2)$$

If we divide $f_k(t_j)$ by the time width of the j-th age, Δt_j, we obtain a SFR for that age (note that VESPA's high-resolution models are computed assuming that the SFRs of galaxies are constant within each age), normalized to the total amount of mass formed by the galaxies in the k-th bin during their lifetimes

$$\psi_k(t_j) = \frac{\sum_{i=1}^{N_k} m_i(t_j)}{\Delta t_j \sum_{i=1}^{N_k} M_i^T}. \quad (3)$$

We show in Fig. 10 the normalized SFR as a function of the look-back time ($t_{\rm LB}$), for each mass bin, environment and sequence. These SFRs were convoluted with a Gaussian kernel with $\sigma = 500$ Myr. We assume all galaxies started their star formation process at $t_{\rm LB} = 14$ Gyr. Clearly, the SFH depends on stellar mass, sequence and environment. In general, we observe that, in the last ~4 Gyr, as was expected, SFS galaxies have been the most actively star forming, followed in a decreasing mode by GV and PS. Another overall conclusion from Fig. 10 is that the more massive the galaxies, the earlier they formed most of their stellar mass. An indication of effects of the environment in the history of star formation in galaxies is evident for GV galaxies: they have SFRs that become more similar to those of PS galaxies as we move from the field to higher density environments.

[3] VESPA models label the most recent age as 0 and the oldest as 15.

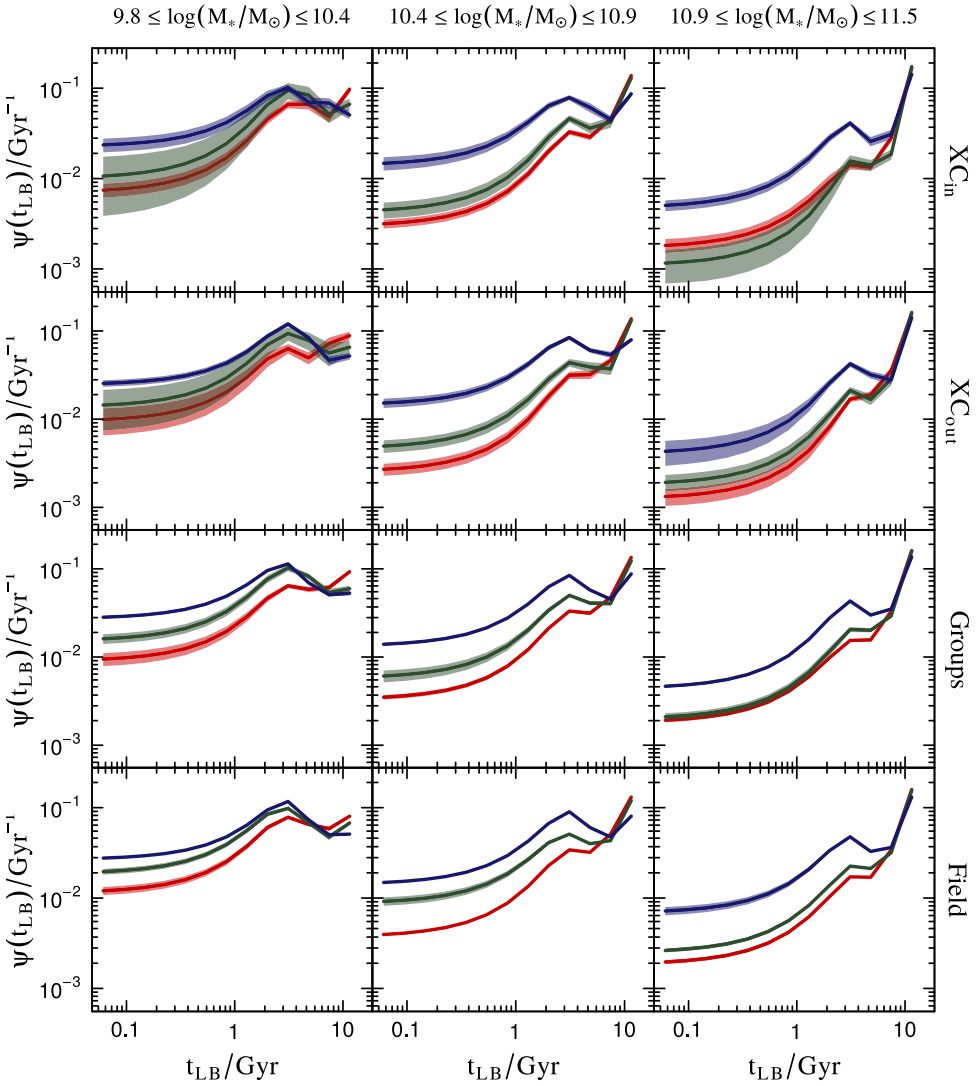

Figure 10. The SFR normalized to the total mass formed throughout the history of the Universe as a function of the lookback time (see equation 3) for a stacking of galaxies as described in the text. All functions shown have been convoluted with a Gaussian kernel. Columns correspond to different stellar masses, as quoted at the top. Rows correspond to different environments, as quoted on the right. Error bars were computed using the bootstrap resampling technique. Colours are as in Fig. 4

The normalized SFRs shown in Fig. 10 rapidly decay with cosmic time during the last ∼4 Gyr, and can be well described by a decaying (growing) exponential function of cosmic (lookback) time from $t_{\rm LB} \sim 4$ Gyr to the present

$$\psi(t_{\rm LB}) = A\ \exp\left(\frac{t_{\rm LB}}{\tau_{\rm q}}\right). \qquad (4)$$

We associate the characteristic time-scale, $\tau_{\rm q}$, to a quenching time. We show in Fig. 11 examples of these normalized SFRs and the best-fitting exponential models (equation 4). Best-fitting parameters for all environments, sequences and mass bins are quoted in Table 1.

We show in Fig. 12, for each environment and sequence, the quenching time and the amplitude of the normalized SFR in the last 4 Gyr as a function of the stellar mass. In general, quenching times are longer for SFS galaxies and shorter for PS galaxies. With the exception of PS galaxies in the inner regions of X-ray clusters, all sequences show quenching times that decrease with increasing mass. It is worth noticing that the quenching times of the PS and the GV of galaxies in clusters are very similar. Regarding the amplitude

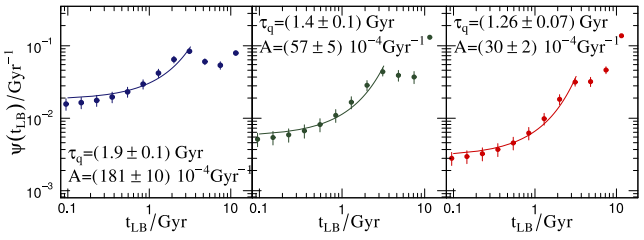

Figure 11. The normalized SFR as a function of the lookback time for intermediate-mass galaxies at the outskirts of X-ray clusters (second column, second row of Fig. 10). Left-hand panel: SFS. Central panel: GV. Right-hand panel: PS. Solid lines are the best-fitting function of the form of equation (4). Inside each panel, we quote the quenching time $\tau_{\rm q}$ and the amplitude A.

of the normalized SFR, the largest values correspond to SFS, intermediate values to GV and the smallest values to PS. All sequences have a decreasing trend with mass. This effect is stronger for the SFS. An environmental dependence of the amplitude of the SFR

Table 1. Best-fitting parameters of the form in equation (4) to the last 4 Gyr of the SFRs in Fig. 10.

Environment	Stellar mass bin	Star forming sequence A (10^{-4}Gyr^{-1})	Star forming sequence τ_q (Gyr)	GV A (10^{-4}Gyr^{-1})	GV τ_q (Gyr)	Passive sequence A (10^{-4}Gyr^{-1})	Passive sequence τ_q (Gyr)
Field	1	306 ± 2	2.12 ± 0.01	237 ± 8	2.03 ± 0.07	150 ± 7	1.78 ± 0.06
	2	170 ± 1	1.74 ± 0.01	121 ± 5	2.09 ± 0.07	46 ± 1	1.45 ± 0.02
	3	93 ± 4	1.89 ± 0.05	30 ± 1	1.48 ± 0.02	22 ± 1	1.49 ± 0.02
Groups	1	310 ± 5	2.14 ± 0.05	184 ± 11	1.7 ± 0.1	115 ± 8	1.7 ± 0.1
	2	162 ± 3	1.78 ± 0.02	78 ± 5	1.63 ± 0.06	40 ± 1	1.40 ± 0.03
	3	53 ± 1	1.40 ± 0.02	22 ± 1	1.36 ± 0.05	22 ± 1	1.52 ± 0.03
XC_{out}	1	271 ± 12	2.0 ± 0.1	175 ± 37	1.8 ± 0.3	121 ± 18	1.8 ± 0.2
	2	181 ± 10	1.9 ± 0.1	57 ± 5	1.4 ± 0.1	30 ± 2	1.26 ± 0.07
	3	55 ± 7	1.5 ± 0.1	21 ± 2	1.3 ± 0.1	14 ± 2	1.24 ± 0.07
XC_{in}	1	267 ± 22	2.2 ± 0.2	135 ± 36	1.5 ± 0.3	88 ± 7	1.5 ± 0.1
	2	184 ± 13	2.0 ± 0.1	52 ± 5	1.4 ± 0.1	36 ± 2	1.34 ± 0.05
	3	59 ± 4	1.5 ± 0.1	12 ± 2	1.2 ± 0.1	20 ± 2	1.5 ± 0.1

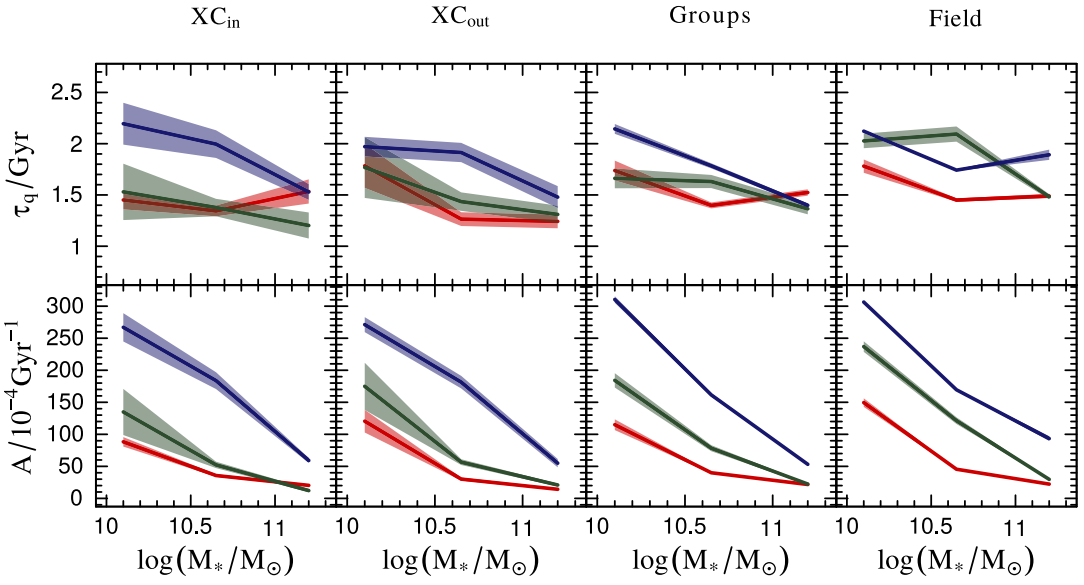

Figure 12. The stellar mass dependence of the best-fitting quenching time τ_q (upper panels) and amplitude A (lower panels) to the last 4 Gyr of the SFRs in Fig. 10. Panels correspond to different environments, from left to right: inner regions of X-ray clusters, outer regions of X-ray clusters, groups, and field. Colours are as in Fig. 4.

for GV galaxies is seen in this figure: moving from the field to the inner regions of clusters, it becomes more similar to the PS values.

The effects of the environment on star formation are more clearly seen in Fig. 13, where we plot the quenching time and the amplitude of the normalized SFRs as a function of the environment. This figure shows that the GV is the sequence that has the most consistent trend with the environment: regardless the mass bin, both the quenching time and the amplitude decay monotonically with increasing density environment. This consistency is not seen for SFS and PS.

From Figs 12 and 13, we were able to conclude that the quenching of the star formation in SFS galaxies is primarily determined by their mass, whereas for GV galaxies it is more sensitive to the environment. The quenching time of PS galaxies appears to be less dependent on mass and environment.

4 DISCUSSION AND CONCLUSIONS

To shed light on the impact of internal and external quenching mechanisms upon galaxies, in this paper we compare properties of star-forming, passive and transition galaxies in four discrete environments: field, groups as a representative of intermediate-mass systems, and X-ray clusters, the most massive virialized systems in the Universe, distinguishing between their inner and outer regions. We construct samples of galaxies in these environments that are bound to have similar redshift distributions out of the SDSS. We classify galaxies into three sequences: passive, GV and star forming, by means of their UV-optical colour $^{0.1}(NUV - r)$. We study a number of galaxy properties: stellar mass, morphology, sSFR and the history of star formation.

Our main findings can be summarized as:

(i) Regarding the morphological classification, as is well established in the literature, GV galaxies have intermediate morphologies. We show that this appears to be independent of the environment, with the possible exception of the inner regions of X-ray clusters where few green spirals are found.

(ii) When comparing GV stellar masses across environments, field galaxies tend to be more massive than in other environments.

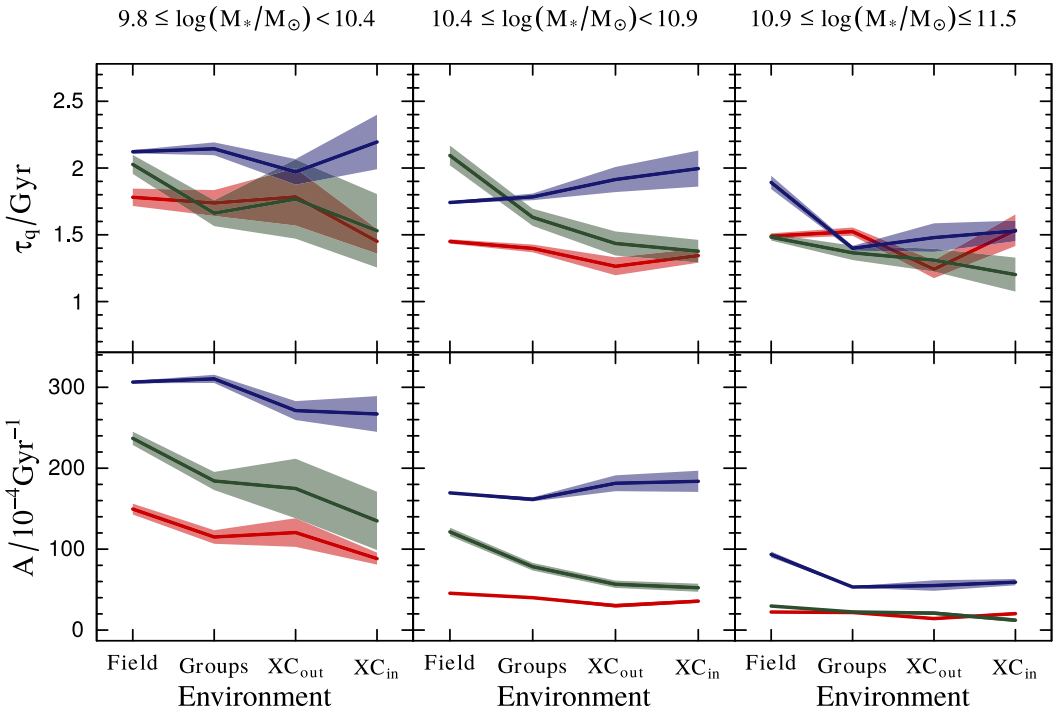

Figure 13. The environment dependence of the best-fitting quenching time τ_q (upper panels) and amplitude A (lower panels) to the last 4 Gyr of the SFRs in Fig. 10. Panels correspond to different stellar mass bins, as quoted at the top. Colours are as in Fig. 4.

The environment that has the largest fraction of low-mass GV galaxies is the outskirts of clusters. If internal quenching is more efficient in massive galaxies, the environment should play a central role in quenching lesser massive galaxies, as our results suggest.

(iii) In contrast to the growing (decaying) trend of the abundance of PS (SFS) galaxies as a function of stellar mass, seen in all environments, the abundance of GV galaxies is almost constant, with the exception of the field. On average, GV galaxies account for ∼20 per cent of all galaxies in groups and X-ray clusters. The field differs from the other environments in that it has a clear lack of $\sim 10^{10}$ $M_\odot$ GV and PS galaxies. This is another indication that high-density environments are needed to transform lower mass galaxies. At the high-mass end, we observe that the fraction of galaxies in the PS is similar for the three densest environments, suggesting that, beyond a certain (high) density threshold, efficiency in quenching galaxies is independent of environment. Similarly, Martínez, Coenda & Muriel (2008) suggested that, above a certain cluster mass, galaxies in clusters experience the same physical processes acting with similar relative effectiveness, thus producing a saturation in the mass–colour relationship.

(iv) When analysing the relationship between the sSFR and the stellar mass, we find that GV galaxies lie far off the main sequence, and closer to PS galaxies. We find that the sSFR–stellar mass relation does not depend on environment.

(v) Using VESPA data, we find that the stacked SFH in the inner regions of galaxies depends on sequence and environment. In general, over the last ∼4 Gyr, GV galaxies have SFRs intermediate between SFS and PS galaxies. As denser environments are considered, the history of star formation of GV galaxies becomes more similar to that of PS galaxies.

(vi) Using a simple decaying exponential model to describe the SFR of galaxies in the last 4 Gyr, we estimate the quenching time and amplitude of the SFR as a function of sequence and environment. As expected, the longest quenching times and largest amplitudes correspond to SFS. PS galaxies have typically the shortest quenching times and smallest amplitudes. In most cases, GV galaxies have intermediate values. The GV is the sequence that has the clearest and most consistent dependence on the environment: both the quenching time and the amplitude decrease with increasing environment density.

Our results indicate that external quenching sources have an important role in galaxy evolution. The relative impact upon galaxies of internal and external quenching processes clearly depends on environment. Since field galaxies are less affected by environmental processes, internal quenching should be their main driver of transformation. As we move from the field to denser environments, the physical mechanisms responsible for external quenching become more efficient, as can be seen from the higher fraction of PS galaxies in these environments. Quenching times in these denser environments are shorter than in the field, and the physical processes that determine external quenching can account for these differences. The impact of dense environments, such as groups, has been reported by Rasmussen et al. (2012), favouring average quenching time-scales of $\gtrsim$2 Gyr and suggesting the simultaneous action of tidal interactions and starvation. These time-scales are close to our findings and larger than those <1 Gyr found by Crossett et al. (2017).

The fact that the fraction of transition galaxies remains roughly constant with stellar mass in dense environments may be explained in terms of two opposite effects: an increase in the likelihood and/or relative strength of quenching processes as M_* increases, and a decrement with M_* of the number of galaxies in the SFS to be quenched.

ACKNOWLEDGEMENTS

We thank the anonymous referee for comments and suggestions that improved this paper.

This paper was partially supported by CONICET grants PIP 11220130100365CO and 11220120100492CO, and grants from SeCyT, Universidad Nacional de Córdoba, Argentina.

Funding for the SDSS-IV has been provided by the Alfred P. Sloan Foundation, the US Department of Energy Office of Science and the Participating Institutions. SDSS-IV acknowledges support and resources from the Center for High-Performance Computing at the University of Utah. The SDSS web site is www.sdss.org. SDSS-IV is managed by the Astrophysical Research Consortium for the Participating Institutions of the SDSS Collaboration including the Brazilian Participation Group, the Carnegie Institution for Science, Carnegie Mellon University, the Chilean Participation Group, the French Participation Group, Harvard-Smithsonian Center for Astrophysics, Instituto de Astrofísica de Canarias, the Johns Hopkins University, Kavli Institute for the Physics and Mathematics of the Universe (IPMU)/University of Tokyo, Lawrence Berkeley National Laboratory, Leibniz Institut für Astrophysik Potsdam (AIP), Max-Planck-Institut für Astronomie (MPIA Heidelberg), Max-Planck-Institut für Astrophysik (MPA Garching), Max-Planck-Institut für Extraterrestrische Physik (MPE), National Astronomical Observatories of China, New Mexico State University, New York University, University of Notre Dame, Observatário Nacional/MCTI, The Ohio State University, Pennsylvania State University, Shanghai Astronomical Observatory, United Kingdom Participation Group, Universidad Nacional Autónoma de México, University of Arizona, University of Colorado Boulder, University of Oxford, University of Portsmouth, University of Utah, University of Virginia, University of Washington, University of Wisconsin, Vanderbilt University and Yale University.

GALEX is a NASA Small Explorer, launched in 2003. We acknowledge NASA"s support for construction, operation and science analysis for the *GALEX* mission, developed in cooperation with the Centre National d'Etudes Spatiales of France and the Korean Ministry of Science and Technology.

REFERENCES

Abadi M. G., Moore B., Bower R. G., 1999, MNRAS, 308, 947
Abazajian K. N. et al., 2009, ApJS, 182, 543
Abramson L. E., Kelson D. D., Dressler A., Poggianti B., Gladders M. D., Oemler A. Jr, Vulcani B., 2014, ApJ, 785, L36
Baldry I. K., Glazebrook K., Brinkmann J., Ivezić Ž., Lupton R. H., Nichol R. C., Szalay A. S., 2004, ApJ, 600, 681
Balogh M. L., Schade D., Morris S. L., Yee H. K. C., Carlberg R. G., Ellingson E., 1998, ApJ, 504, L75
Bamford S. P. et al., 2009, MNRAS, 393, 1324
Beers T. C., Flynn K., Gebhardt K., 1990, AJ, 100, 32
Bell E. F. et al., 2004, ApJ, 608, 752
Bohringer H. et al., 2000, ApJS, 129, 435
Brinchmann J., Charlot S., White S. D. M., Tremonti C., Kauffmann G., Heckman T., Brinkmann J., 2004, MNRAS, 351, 1151
Bruzual G., Charlot S., 2003, MNRAS, 344, 1000
Calzetti D., Armus L., Bohlin R. C., Kinney A. L., Koornneef J., Storchi-Bergmann T., 2000, ApJ, 533, 682
Chilingarian I. V., Zolotukhin I. Y., 2012, MNRAS, 419, 1727
Cimatti A. et al., 2013, ApJ, 779, L13
Coenda V., Muriel H., 2009, A&A, 504, 347
Cortese L., 2012, A&A, 543, A132
Crain R. A. et al., 2015, MNRAS, 450, 1937
Crossett J. P., Pimbblet K. A., Jones D. H., Brown M. J. I., Stott J. P., 2017, MNRAS, 464, 480
Di Matteo T., Springel V., Hernquist L., 2005, Nature, 433, 604
Díaz E., Zandivarez A., Merchán M. E., Muriel H., 2005, ApJ, 629, 158
Elbaz D. et al., 2011, A&A, 533, A119
Faber S. M. et al., 2007, ApJ, 665, 265
Fang J. J., Faber S. M., Salim S., Graves G. J., Rich R. M., 2012, ApJ, 761, 23
Feldmann R. et al., 2006, MNRAS, 372, 565
Gunn J. E., Gott J. R. I., 1972, ApJ, 176, 1
Hasinger G., 2008, A&A, 490, 905
Huchra J. P., Geller M. J., 1982, ApJ, 257, 423
Im M. et al., 2002, ApJ, 571, 136
Johnson B. D. et al., 2006, ApJ, 644, L109
Kauffmann G. et al., 2003, MNRAS, 341, 33
Kaviraj S., Peirani S., Khochfar S., Silk J., Kay S., 2009, MNRAS, 394, 1713
Kawata D., Mulchaey J. S., 2008, ApJ, 672, L103
Kormendy J., Kennicutt R. C., Jr, 2004, ARA&A, 42, 603
Larson R. B., Tinsley B. M., Caldwell C. N., 1980, ApJ, 237, 692
Leitner S. N., 2012, ApJ, 745, 149
Limber D. N., Mathews W. G., 1960, ApJ, 132, 286
Lintott C. J. et al., 2008, MNRAS, 389, 1179
Lintott C. et al., 2011, MNRAS, 410, 166
Marasco A., Fraternali F., Binney J. J., 2012, MNRAS, 419, 1107
Maraston C., 2005, MNRAS, 362, 799
Martin D. C. et al., 2007, ApJS, 173, 342
Martínez H. J., Coenda V., Muriel H., 2008, MNRAS, 391, 585
Masters K. L. et al., 2010, MNRAS, 405, 783
Masters K. L. et al., 2011, MNRAS, 411, 2026
McConnell N. J., Ma C.-P., 2013, ApJ, 764, 184
Mendez A. J., Coil A. L., Lotz J., Salim S., Moustakas J., Simard L., 2011, ApJ, 736, 110
Moore B., Katz N., Lake G., Dressler A., Oemler A., 1996, Nature, 379, 613
Moore B., Lake G., Quinn T., Stadel J., 1999, MNRAS, 304, 465
Muriel H., Coenda V., 2014, A&A, 564, A85
Nandra K. et al., 2007, ApJ, 660, L11
Peng Y.-j. et al., 2010, ApJ, 721, 193
Popesso P., Böhringer H., Brinkmann J., Voges W., York D. G., 2004, A&A, 423, 449
Rasmussen J., Mulchaey J. S., Bai L., Ponman T. J., Raychaudhury S., Dariush A., 2012, ApJ, 757, 122
Salim S., 2014, Serb. Astron. J., 189, 1
Salim S. et al., 2007, ApJS, 173, 267
Salim S., Fang J. J., Rich R. M., Faber S. M., Thilker D. A., 2012, ApJ, 755, 105
Schawinski K., Thomas D., Sarzi M., Maraston C., Kaviraj S., Joo S.-J., Yi S. K., Silk J., 2007, MNRAS, 382, 1415
Schawinski K. et al., 2009, MNRAS, 396, 818
Schawinski K. et al., 2014, MNRAS, 440, 889
Schaye J. et al., 2015, MNRAS, 446, 521
Schiminovich D. et al., 2007, ApJS, 173, 315
Schlegel D. J., Finkbeiner D. P., Davis M., 1998, ApJ, 500, 525
Silverman J. D. et al., 2008, ApJ, 675, 1025
Strateva I. et al., 2001, AJ, 122, 1861
Strauss M. A. et al., 2002, AJ, 124, 1810
Takamiya M., Kron R. G., Kron G. E., 1995, AJ, 110, 1083
Thilker D. A. et al., 2010, ApJ, 714, L171
Tojeiro R., Heavens A. F., Jimenez R., Panter B., 2007, MNRAS, 381, 1252
Tojeiro R., Wilkins S., Heavens A. F., Panter B., Jimenez R., 2009, ApJS, 185, 1
Trayford J. W., Theuns T., Bower R. G., Crain R. A., Lagos C. del P., Schaller M., Schaye J., 2016, MNRAS, 460, 3925
Weiner B. J. et al., 2005, ApJ, 620, 595
Willmer C. N. A. et al., 2006, ApJ, 647, 853
Wyder T. K. et al., 2007, ApJS, 173, 293
York D. G. et al., 2000, AJ, 120, 1579
Zandivarez A., Martínez H. J., 2011, MNRAS, 415, 2553

This paper has been typeset from a TEX/LATEX file prepared by the author.